BIOCHEMISTRY

Sorbate induces lysine sorbylation through noncanonical activities of class I HDACs to regulate the expression of inflammation genes

Yi-Cheng Sin[1,2], Breann Abernathy[1], Zuo-fei Yuan[3], Jason L. Heier[1], Justin E. Gonzalez[1], Laurie L. Parker[1], Douglas G. Mashek[1,4,5]*, Yue Chen[1]*

Environmental factors may affect gene expression through epigenetic modifications of histones and transcription factors. Here, we report that cellular uptake of sorbate, a common food preservative, induces lysine sorbylation (Ksor) in mammalian cells and tissue mediated by the noncanonical activities of class I histone deacetylases (HDAC1-3). We demonstrated that HDAC1-3 catalyze sorbylation upon sorbate uptake and desorbylation in the absence of sorbate both in vitro and in cells. Sorbate uptake in mice livers significantly induced histone Ksor, correlating with decreased expressions of inflammation-response genes. Accordingly, sorbate treatment in macrophage RAW264.7 cells upon lipopolysaccharide (LPS) stimulation dose-dependently down-regulated proinflammatory gene expressions and nitric oxide production. Proteomic profiling identified RelA, a component of the NF-κB complex, and its interacting proteins as bona fide Ksor targets and sorbate treatment significantly decreased NF-κB transcriptional activities in response to LPS stimulation in RAW264.7 cells. Together, our study demonstrated a noncanonical mechanism of sorbate uptake in regulating epigenetic histone modifications and inflammatory gene expression.

INTRODUCTION

Environmental chemicals regulate cellular activities and organismal functions through multifaceted biochemical processes (*1*–*4*). Mechanistic understanding of these processes is instrumental in properly evaluating their physiological impact on human health and developing potential therapeutic interventions. Sorbate is a six-carbon polyunsaturated fatty acid widely used as a chemical preservative in processed food, personal cosmetic products, and pharmaceutical formulations to prevent microbial contamination and ensure product safety (*5*–*7*). Earlier studies in animal and cell models suggested that sorbate uptake had very low cytotoxicity and did not have carcinogenetic activity (*5*–*9*). Yet, more recent studies applying mutagenic and chromosome analysis as well as transcriptome and chromatin analysis showed that sorbate treatment could be potentially genotoxic and affect gene expression in cells and tissues (*10*–*15*). Notably, sorbate treatment may affect fatty acid oxidation pathways and corresponding gene expression in mouse liver (*15*). Thus, the accumulating evidence suggests that chronic sorbate uptake led to changes in gene expression, suggesting a nontrivial role of sorbate uptake in mediating epigenetic dynamics. Given the wide usage of this chemical in food preservation, it is pivotal to uncover the molecular mechanism of sorbate-mediated dynamics of transcription regulation and its potential impact on human physiology.

Gene transcription and cell signaling are intimately linked to chemicals in the cellular microenvironment through protein posttranslational modifications (PTMs) (*16*–*18*). Covalent modifications of proteins through enzymatic or nonenzymatic processes may alter protein structure, enzymatic activity, or protein-protein interaction. Histones and transcription factors are critical targets of active environmental chemicals as the change in their activities profoundly affects the transcriptional landscape in cells and tissues. With about 500 types of protein modifications reported to date, more than 20 types of modifications have been discovered on histones, and their characterization reveals differential epigenetic effects and intimate links to cellular metabolism (*19*, *20*).

Histone lysine short-chain acylation is a family of protein PTMs and histone epigenetic marks in mammalian cells (*1*). Starting from lysine propionylation and butyrylation to more recently reported lysine lactylation, these chemical modifications demonstrated that metabolic-linked fatty acids could be activated in situ and served as coenzymes for acyltransferases that participate in diverse transcription and signaling processes (*21*–*24*). The consequential covalent modification of histones and nonhistones has been found to induce protein interactions and regulate enzymatic or transcriptional activities to affect the cellular physiological response to energy and nutrients (*24*–*26*). Inspired by these studies, we showed that the cellular uptake of sorbate, the widely used chemical preservative, induced novel lysine sorbylation (Ksor) in cells and tissues. We demonstrated that Ksor was dynamically regulated by class I lysine deacetylases (HDAC1-3) that harbor noncanonical functions as either sorbyltransferase or desorbylase depending on the sorbate availability. An increase in Ksor abundance correlated with decreased inflammatory gene expression in mouse liver and cultured macrophage RAW264.7 cells. Global proteomic analysis with immunoprecipitation and liquid chromatography–mass spectrometry (LC-MS) analysis revealed widespread Ksor induced by sorbate treatment and identified RelA (p65), a member of the nuclear factor κB (NF-κB) complex, as a Ksor target for regulating its transcriptional activities. These studies demonstrated Ksor as a new histone epigenetic mark and a novel mechanism in sorbate-mediated regulation of inflammation gene expression.

[1]Department of Biochemistry, Molecular Biology and Biophysics, University of Minnesota Twin Cities, Minneapolis, MN, USA. [2]Bioinformatics and Computational Biology Program, University of Minnesota Twin Cities, Minneapolis, MN, USA. [3]Center for Proteomics and Metabolomics, St. Jude Children's Research Hospital, Memphis, TN, USA. [4]Department of Medicine, Division of Diabetes, Endocrinology, and Metabolism, University of Minnesota Twin Cities, Minneapolis, MN, USA. [5]Institute for the Biology of Aging and Metabolism, University of Minnesota Twin Cities, Minneapolis, MN, USA.
*Corresponding author. Email: yuechen@umn.edu (Y.C.); dmashek@umn.edu (D.G.M.)

RESULTS

Sorbate uptake induces Ksor, a novel histone epigenetic mark

To determine whether sorbate uptake induced endogenous Ksor, we performed histone extraction and in-gel digestion to sorbate-treated HCT116 human cell line (Fig. 1A). We confidently identified histone peptides with a mass shift of 94.0419 (C6H6O) on lysine residues that matched the expected mass shift of sorbylation on lysine [an example of histone H4 peptide GLGK(sorbylation)GGAK-(acetylation)R was shown] (Fig. 1B). To validate the identified Ksor, we performed high-resolution LC–tandem MS (MS/MS) analysis with high-performance liquid chromatography (HPLC) co-elution assay on synthetic peptides with identical sequences and expected modifications as endogenous histone peptides. We observed that the high-resolution MS and MS/MS spectra of the endogenous peptides matched those of the synthetic peptides with very close retention times. Upon mixing synthetic peptides with endogenous peptides, they co-eluted perfectly. These data confidently validated the identification of Ksor in cells. To further confirm that exogenous sorbate drove Ksor, we treated the cells with either regular sorbic acid or heavy isotope–labeled $^{13}C_2$-sorbic acid (Fig. 1C). The treatment of $^{13}C_2$-sorbate led to the identification of $^{13}C_2$-Ksor without the identification of unlabeled Ksor peptides. Comparing precursor ion MS and fragment ion MS/MS spectra of both light and heavy Ksor peptide showed expected mass shifts on precursor ions as well as fragment ions bearing the modification. These data suggested that exogenous sorbate uptake induced histone Ksor.

To comprehensively identify histone Ksor, we extracted histones from the sorbate-treated human and mouse cell lines as well as liver tissue from mice that were fasted overnight and then fed diets containing 0.1 and 0.5% (wt %) of sorbate for 12 weeks and performed in-gel digestion for LC-MS analysis (Fig. 1D). This level of inclusion in the diet was designed considering the range of 0 to 25 mg/kg of body weight for acceptable daily intake (ADI) for sorbate based on the guidelines from the World Health Organization and dose conversion between animals and human (see the Materials and Methods) (*27*, *28*). We identified a total of 48, 36, and 18 Ksor sites on core histones from 293T cells, RAW264.7 cells, and mouse livers, respectively (fig. S1 to S3 and data S1). These histone Ksor sites were located close to the N terminal of the core histones, which overlapped with well-characterized histone acetylation and methylation sites, suggesting a potential role of Ksor in regulating gene expression through epigenetic mechanisms (Fig. 1D). It is also likely that Ksor sites on core histones may be identified in other histone regions with increasing sequence coverage and sensitivity of proteomic analysis.

To study the dynamic of the Ksor induced by dietary sorbic acid, we generated a pan anti-sorbylation antibody. We validated the specificity of the Ksor antibody with dot blots against the unmodified peptides, sorbylated peptides, and peptides bearing previously reported acylations with homologous structures, including lysine acetylation and crotonylation (Fig. 2A). Our data suggested that the pan-antibody had high sensitivity and specificity for Ksor. Using this antibody, we evaluated the induction of histone sorbylation upon sorbate treatment in various types of common cell lines, including HepG2, human embryonic kidney 293T, and RAW264.7 (Fig. 2B). Histone sorbylation was readily induced across different cell lines, suggesting that sorbate uptake could induce Ksor in cell culture without affecting overall histone lysine acetylation. To determine the temporal dynamics of sorbylation at a whole-cell level, we treated the RAW264.7 cells with 2 or 5 mM sorbate at various times. We observed the induction of Ksor with increasing treatment dosages and treatment times (fig. S4). To determine whether sorbate uptake in mice could induce Ksor in tissues, we orally gavaged mice with sorbate equivalent to what would be consumed daily with the 0.5% sorbate diet and harvested mouse livers after various times following the treatment for histone extraction and Western blotting. We observed that the histone sorbylation significantly increased in 2 hours after consuming a diet with sorbate without apparently affecting lysine acetylation compared to control diet (Fig. 2C and fig. S5). This result suggested that the Ksor could be induced acutely upon sorbate uptake in cultured cells and mouse tissues at physiological doses.

We then applied EpiProfile analysis to determine the site-specific dynamics and fractional abundance of histone Ksor compared to common histone epigenetic marks. To this end, 293T cells treated with or without 10 mM potassium sorbate overnight were lysed for acid-based histone extraction. Extracted histone proteins were propionylated and then digested by trypsin. Peptides were analyzed by data-independent LC-MS analysis following the previously established workflow (*29*). Data were analyzed by EpiProfile 2.1 with label-free quantification. Our data showed that sorbate treatment significantly induced histone H3K18 and H3K23 sorbylation with a fractional abundance of around 0.01 and 0.03%, respectively (fig. S6). Among common histone epigenetic marks, sorbate treatment did not lead to significant changes in fractional abundance except for slight increases in histone H3K18 acetylation and H3.3K27 trimethylation (not significant with Benjamini-Hochberg correction) (fig. S6). The fractional abundance of histone sorbylation was comparable to some histone marks with low abundance such as H3K4 trimethylation and H3.1K27 acetylation but much lower than abundant histone marks such as H3K23 and H4K16 acetylation (data S2).

Class I histone deacetylase regulates Ksor dynamics

To determine the regulators of Ksor dynamics, we hypothesized that certain members of histone lysine deacetylases (HDACs) known to have promiscuous enzymatic activity could function as lysine desorbylases to remove Ksor as previously reported for other lysine short chain acylations (*30*–*32*). To this end, we performed a chemical screening with various HDAC inhibitors that have been well characterized to target different families of HDACs. We expected that the inhibition of HDAC enzymes in cells that functioned as the major lysine desorbylase could retain the level of histone sorbylation after the sorbate removal. To this end, 293T cells were pulsed with sorbate overnight to induce histone sorbylation and then chased with medium without sorbate and containing various types of HDAC inhibitors or vehicles. Last, we harvested cells for histone extraction and Western blotting after 5 hours of inhibitor treatments (Fig. 3B). Our data showed that without inhibitor treatments, the abundance of Ksor diminished quickly in 5 hours (Fig. 3B, lanes 2 versus 3). Treatments with different inhibitors for class 1, 2, and 4 HDACs retained Ksor levels, but the class 3 HDAC inhibitor was not as efficient (Fig. 3B, lanes 4 and 5 versus lane 6). Inhibition of class 4 HDAC, which only includes HDAC11, did not retain Ksor (Fig. 3B, lane 9). Class 2 HDACs could be classified into class 2a (HDAC4, HDAC5, HDAC7, and HDAC9) and class 2b (HDAC6 and HDAC10). Treatment with a class 2a inhibitor failed to retain histone sorbylation, while the inhibitor toward classes 1 and 2b was highly effective (Fig. 3B, lanes 7 and 8). Last, treatment with MS275 alone, a highly selective

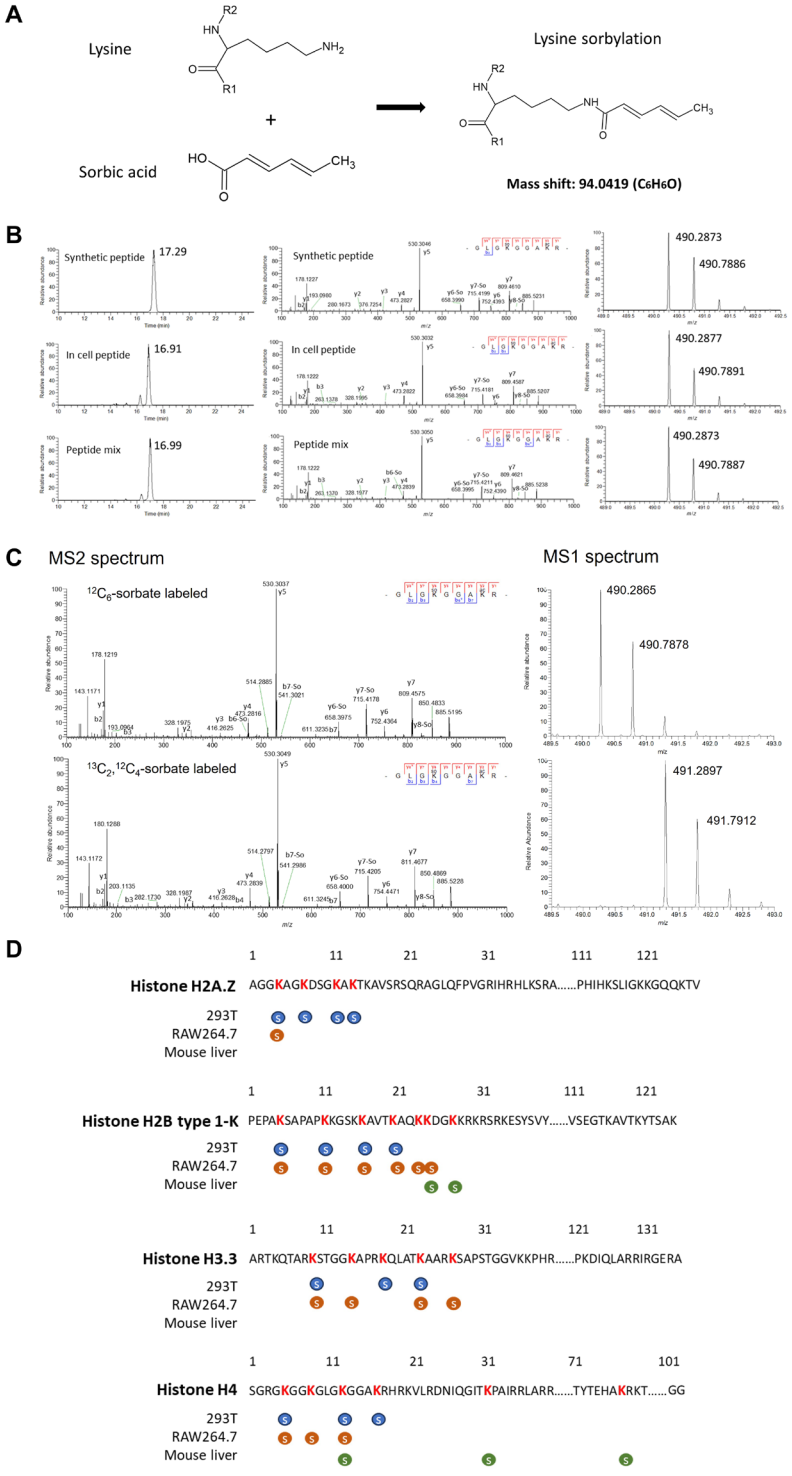

Fig. 1. Identification and validation of dietary sorbic acid–induced Ksor. (**A**) Illustrations for the chemical structures of sorbic acid and the formation of protein Ksor. (**B**) Extracted ion high-performance liquid chromatography (HPLC) chromatograms and MS spectra for the validation of Ksor with HPLC co-elution analysis. Histone H4 K12 sorbylation peptide "GLGK(So)GGAK(Ac)R" was used as an example (So, Ksor; Ac, lysine acetylation). "-So" in MS/MS spectra indicates the neutral loss signal of Ksor. Histones were extracted for HCT116 cells treated with 10 mM of sorbate for 24 hours and subject to SDS–polyacrylamide gel electrophoresis (PAGE) and in-gel digestion by trypsin. Diluted synthetic peptide, endogenous histone peptides from in-gel digestion, and their equal mixture were analyzed with the same HPLC gradient to compare chromatography retention time (left column), MS2 fragmentation (middle column), and peptide MS1 mass/charge ratio (m/z) = 490.2804 to 490.2952 (right column). (**C**) Validation of Ksor with isotopic labeling in HCT116 cells. HCT116 cells were treated with 2 mM $^{13}C_2$-sorbate for 24 hours, and histones were extracted for in-gel tryptic digestion. Peptides were analyzed by LC-MS and compared with Ksor peptides from sorbate-treated HCT116 cells. (**D**) Illustration of representative Ksor sites identified on core histones from the LC-MS analysis of histones extracted from sorbate-treated 293T cells (blue), Raw264.7 cells (orange), and mouse liver tissue (green).

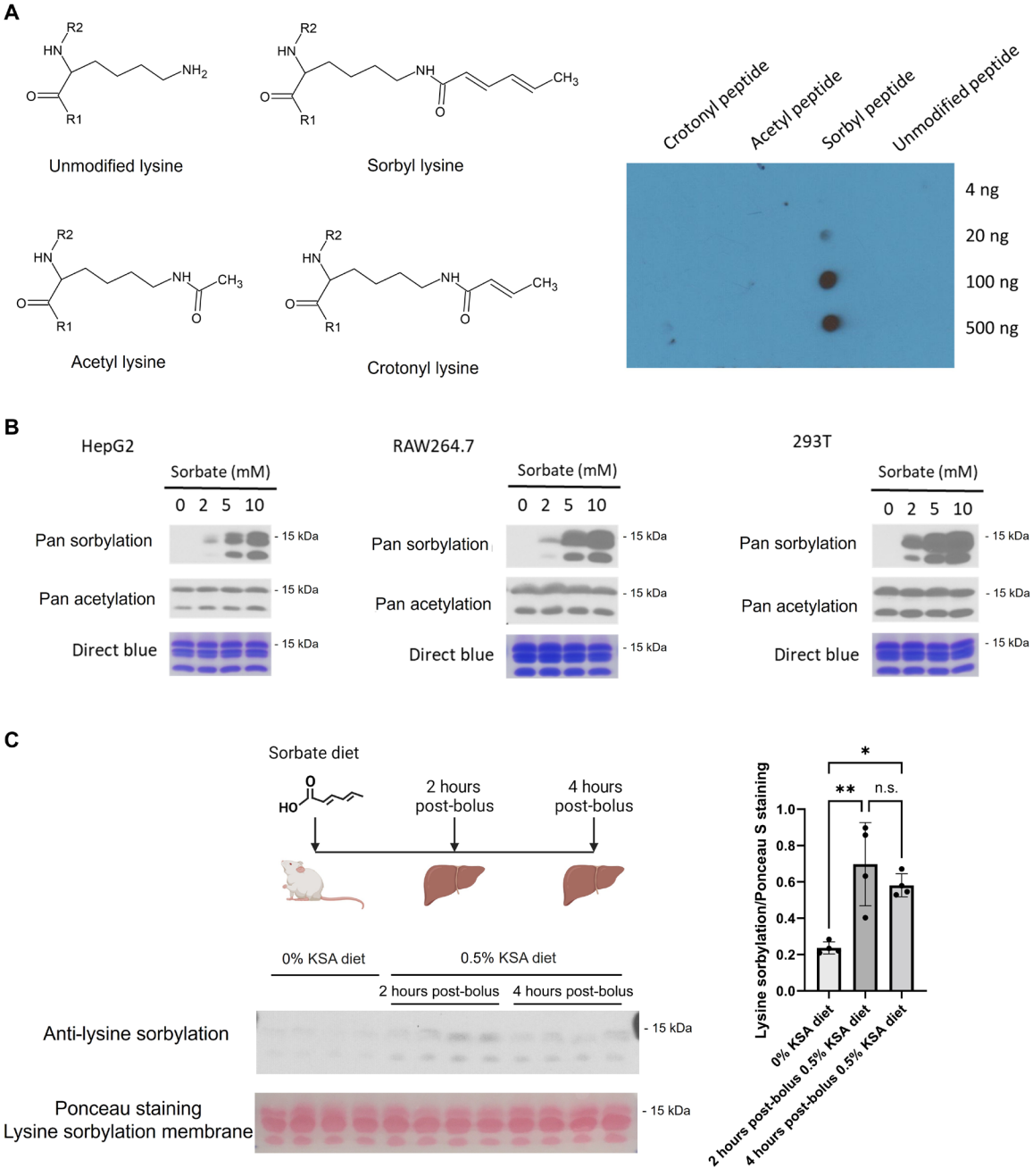

Fig. 2. Dynamics of histone sorbylation in cell models and mouse liver tissues. (**A**) Dot blot assay for the validation of pan anti-Ksor antibody with unmodified peptides or peptides modified with Ksor, acetylation, or crotonylation. (**B**) Western blot analysis of histones extracted from HepG2 (left), Raw264.7 (middle), and 293T cells (right) treated with various concentrations of sorbate for 24 hours. (**C**) Western blot analysis of histones extracted from liver tissues of mice fed with a diet containing 0.5% potassium sorbate (KSA) via oral gavage. Liver tissues were extracted from control mice right away after oral gavage and from mice fed with a sorbate-containing diet 2 or 4 hours post-feeding. Western blotting with pan anti-Ksor antibody and Ponceau staining were quantified with Image J software, and the bar graph quantification was performed with a one-way analysis of variance (ANOVA) test with Tukey's multiple comparisons test (biological replicates, $n = 4$). Error bars represent SD. $^{*}P < 0.05$ and $^{**}P < 0.01$. Created in BioRender (Y. Chen, 2025; https://BioRender.com/o03b638). n.s., not significant.

inhibitor toward HDAC1, HDAC2, and HDAC3, was sufficient to retain histone Ksor level (Fig. 3B, lane 10). We repeated the inhibitor screening in RAW264.7 cells to confirm these findings and observed similar effects (fig. S7). These data suggested that class 1 HDACs, including HDAC1, HDAC2, and HDAC3, were potential major histone desorbylases in cells.

To confirm the histone desorbylase activity of these candidate enzymes, we performed in vitro enzymatic assays. Histones extracted from sorbate-treated 293T cells were incubated with equal concentrations of recombinant HDAC1, HDAC2, and HDAC3 enzymes (Fig. 3C). The result showed that all three enzymes exhibited histone desorbylase activities in vitro. The addition of butyrate, a class I

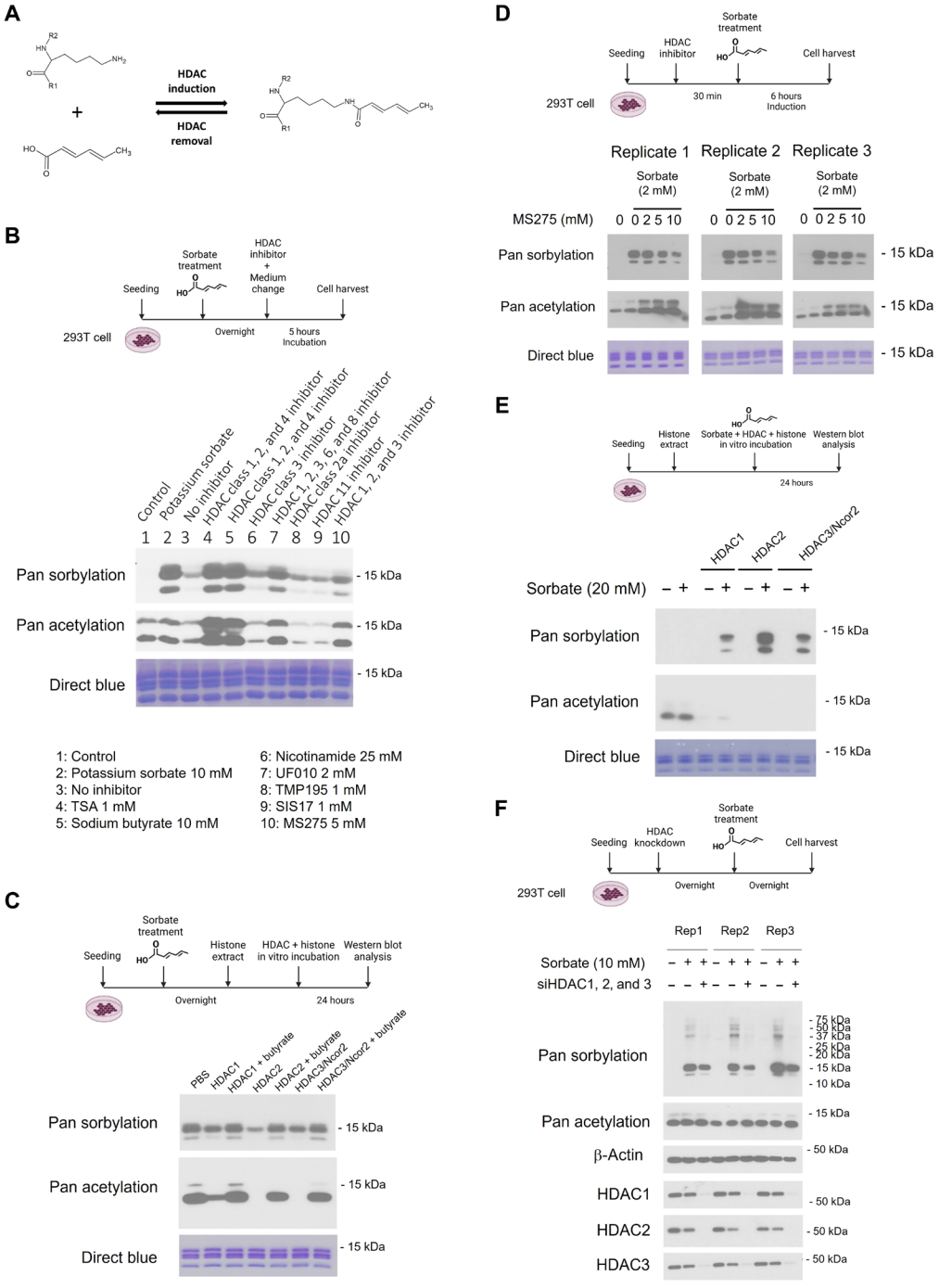

Fig. 3. Regulation of Ksor by class I HDACs. (**A**) Schematic representation of HDAC-mediated Ksor and desorbylation. (**B**) Chemical inhibitor screening with extracted histones to identify a major class of HDACs that remove histone lysine sorbylation in cells. 293T cells were treated with 10 mM sorbate overnight. Sorbate-containing media were replaced with fresh media with or without various chemical inhibitors for 5 hours targeting different classes of HDACs including TSA (1 μM, lane 4), sodium butyrate (10 mM, lane 5), nicotinamide (25 mM, lane 6), UF010 (2 μM, lane 7), TMP195 (1 μM, lane 8), SIS17 (1 μM, lane 9), and MS275 (5 μM, lane 10) (**C**) Enzymatic assay and Western blot analysis demonstrating the in vitro desorbylase activities of class I HDACs (HDAC1-3) with recombinant enzymes and extracted histones from 293T cells treated with or without 10 mM sorbate and 40 mM sodium butyrate for 24 hours. (**D**) Western blotting analysis shows that HDAC inhibitor MS275 treatment dose-dependently inhibited Ksor in the presence of sorbate. 293T cells were treated with various concentrations of MS275 first for 30 min followed by the addition of potassium sorbate (2 mM) for the co-treatment of 6 hours before cell harvesting. (**E**) Enzymatic assay and Western blotting analysis demonstrating the in vitro sorbyltransferase activities of class I HDACs (HDAC1-3) with recombinant enzymes and extracted histones from regular 293T cells with or without sorbate. (**F**) siRNA knockdown and Western blot analysis demonstrating the endogenous activities of class I HDACs (HDAC1-3) in mediating global Ksor. SiRNAs targeting HDAC1, HDAC2, or HDAC3 were pooled and transfected to 293T cells for overnight incubation. Media were then replaced with fresh media with or without 10 mM sorbate treatment for overnight. Created in BioRender (Y. Chen, 2025; https://BioRender.com/a34b274, https://BioRender.com/b79o565, https://BioRender.com/r21b608, and https://BioRender.com/n20b369).

HDAC inhibitor, blocked the enzyme activities of HDAC1, HDAC2, and HDAC3 toward both desorbylation and deacetylation (Fig. 3C). Collectively, our data demonstrated that class I HDACs are major enzymes that regulate histone lysine sorybylation removal and Ksor dynamics.

An interesting observation was made during our studies that inhibitors of HDACs exerted their effects only when sorbate was removed from the media. Unexpectedly, in the presence of sorbate, MS275 (specific inhibitors for HDAC1-3) treatment dose-dependently decreased sorbylation level (Fig. 3D). Inspired by the recent study showing that HDAC6 is a lactyltransferase that catalyzes direct lactylation with only lactate as a substrate (*33*), we hypothesized that HDAC1-3 might act as sorbyltransferase in the presence of sorbate. To test this hypothesis, we first performed an in vitro analysis. Histones extracted from cells without sorbate treatment were subject to incubation with recombinant HDAC1, HDAC2, and HDAC3/NCOR2 complex together with or without sorbate, followed by Western blotting analysis with pan anti-Kac and anti-Ksor antibodies (Fig. 3E). Increasing sorbate concentration dose-dependently increased histone sorbylation by HDAC1-3 in vitro without affecting deacetylation of histones (fig. S8A). Inhibiting deacetylase activities with trichostatin A (TSA) treatment also abolished the sorbyltransferase activities of HDAC1-3 in vitro (fig. S8B). These data suggested that HDAC1-3 enzymes harbor noncanonical catalytic activities that function as sorbyltransferases in the presence of sorbate without apparently affecting their capabilities as deacetylases and such sorbyltransferase activities are dependent on their deacetylase activities. We further confirmed these findings with TSA treatment in 293T cells. Again, our data confirmed that the inhibition of HDAC activities abolished sorbate-induced Ksor while up-regulating lysine acetylation in cells (fig. S9). To more specifically determine whether HDAC1-3 could function as sorbyltransferases in cells, we performed small interfering RNA (siRNA)–mediated knockdown of the three enzymes. Our data showed that the combined knockdown of all three HDACs strongly reduced sorbate-induced Ksor, suggesting that HDAC1-3 were essential to induce a large fraction of Ksor in cells (Fig. 3F). These cell-based and in vitro data demonstrated that HDAC1-3 enzymes efficiently catalyzed reversible sorbyltransfer reactions in the presence of sorbate and desorbylation reactions in the absence of sorbate.

Sorbate uptake regulates proinflammatory gene transcription

To determine how the sorbate uptake may affect endogenous gene expression, we collected mouse liver tissues after 4 hours post–bolus treatment of sorbate diet as done in Fig. 2 and performed RNA sequencing (RNA-seq) analysis. With EdgeR analysis, considering adjusted false discovery rate (FDR) < 0.05 and 2× fold change as significant difference, we identified 295 genes that were significantly increased in expression and 471 genes showing reduced expression upon sorbate administration (Fig. 4, A and B; fig. S10; and data S3). Notably, the expressions of numerous inflammation-related genes were down-regulated (Fig. 4A). We performed annotation enrichment analysis of those differentially expressed genes (DEGs). The inflammatory response pathways and related biological processes were significantly enriched among genes with significantly down-regulated expression in mice given sorbate (Fig. 4C). This result suggested that sorbate uptake significantly reduced the proinflammatory gene transcriptome in mouse liver.

To confirm these findings, we applied quantitative polymerase chain reaction (qPCR) analysis and studied the expression of inflammatory-related genes in RAW264.7 mouse macrophage cells upon sorbate uptake. To this end, cells were pretreated by various doses of potassium sorbate overnight followed by lipopolysaccharide (LPS) stimulation for 3 hours (Fig. 5A). qPCR analysis was performed to examine the expression of the proinflammatory genes, including interleukin-6 (*IL-6*), interleukin-1β (*IL-1*β), interleukin-1α (*IL-1*α), inducible nitric oxide synthase (iNOS) (*Nos2*), and cyclooxygenase-2 (Cox2) (*Ptgs2*). Our data showed that sorbate treatment alone did not induce the expression of proinflammatory genes, whereas LPS treatment strongly induced the expression of proinflammatory gene response, as expected. However, when given with LPS, sorbate dose-dependently attenuated the expression of inflammatory genes (Fig. 5A). We further performed nitric oxide assays to determine the effect of sorbate uptake on nitric oxide production. RAW264.7 cells were pretreated with sorbate at various doses overnight, followed by LPS stimulation (Fig. 5B). These data showed that sorbate treatment also dose-dependently reduced the induction of nitric oxide production following LPS. Together, these data demonstrated that the sorbate uptake down-regulated proinflammatory gene expression in tissue and cell models.

Global proteomic profiling revealed Ksor mediating NF-κB transcriptional activity

To systematically profile global Ksor substrates and identify potential mechanisms for sorbate-dependent anti-inflammatory response in macrophage cells, we performed immunoprecipitation with the pan anti-sorbylation antibody followed by HPLC-MS/MS analysis. Briefly, RAW 264.7 cells were pretreated with 10 mM sorbate overnight and then treated with LPS at 100 ng/ml for 3 hours. Then, the cells were harvested and subjected to lysis and trypsin digestion. The digested peptides were immunoprecipitated with the pan anti-sorbylation antibody for LC-MS analysis (Fig. 6A). We identified over 1600 sites on 908 proteins as Ksor modification substrates (data S4). Bioinformatic analysis showed that Ksor proteins were highly enriched in major cellular pathways including RNA processing, ribosome translation, DNA replication, and cell cycle–related pathways (Fig. 6B). We performed the flanking sequence analysis and observed that lysine sites with serine, proline, and alanine as neighboring residues (+2/−2) were often modified by sorbate, and lysine is the most preferred amino acid beyond two residues surrounding the modification site (Fig. 6C). About 63% of the identified proteins only had one modification site, and nearly 40% were multiply modified with some highly modified proteins bearing more than eight Ksor sites (Fig. 6D). Interaction network analysis identified multiple highly connected Ksor substrate interaction subnetworks related to ribosomal protein translation, pre-mRNA processing, splicing, and cell cycle (fig. S11). Notably, we identified one interaction cluster: RelA (p65) interaction network including p65, Brd4, Stat1, Ncor2, Jun, and Ataxia-telangiectasia Mutated (ATM) (Fig. 6E). Given the critical role of p65 and its associated chromatin complex in mediating proinflammatory gene response, these data suggested a potential role of Ksor in regulating proinflammatory gene expression through modulating p65 transcriptional activities.

To further validate p65 as a HDAC-mediated Ksor target, we performed in vitro enzymatic assays. Unmodified peptides of histones and p65 with sequences surrounding several identified Ksor sites were synthesized and incubated with phosphate-buffered saline (PBS) or sorbate with or without HDAC1, HDAC2, or HDAC3/Ncor2

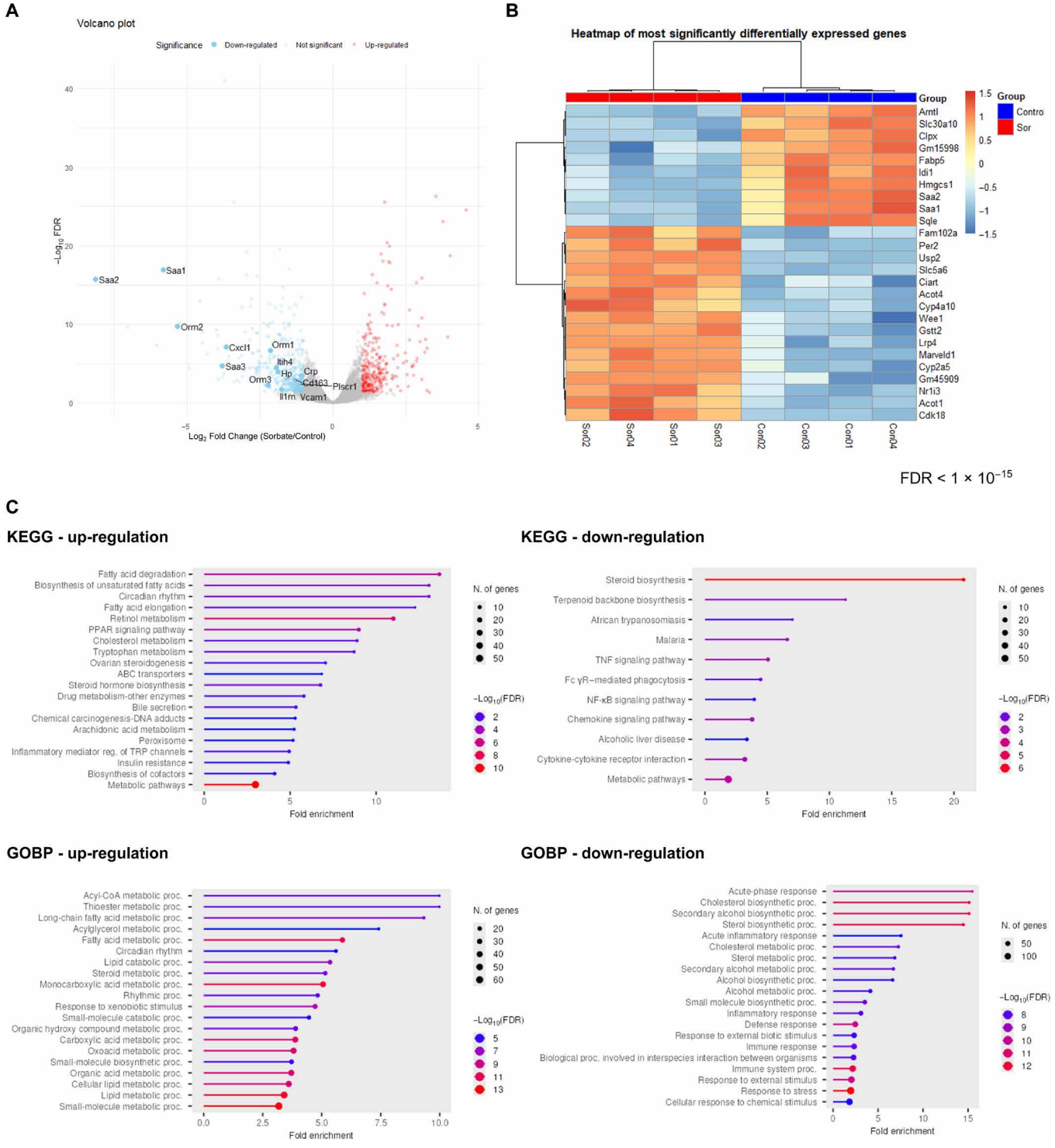

Fig. 4. Sorbate-induced transcriptomic dynamics in mouse liver. Liver tissues were extracted from control mice or mice 4 hours post-feeding with 0.5% potassium sorbate in diet via oral gavage. RNAs were extracted for RNA-seq analysis. (**A**) Volcano plot analysis of gene expression of control and sorbate-treated mouse livers with edgeR (absolute fold change > 2 and FDR < 0.05) representing genes with significant up-regulation (red dots), down-regulation (blue dots), and no significant changes (gray dots). Selected genes in acute inflammatory response pathways (GO:0002526) were labeled. Genes with very high *y*-axis values ($-\log_{10}$ FDR > 45) were not included in the plot for better visualization. (**B**) Heatmap and hierarchical clustering analysis of the most differentially expressed genes (DEGs; FDR < 1×10^{-15}) between control and sorbate-treated mouse livers. Scale bar represented standardized (*z*-score) values (**C**) Gene Ontology annotation enrichment analysis for significantly up-regulated (left column) or down-regulated (right column) genes upon sorbate treatment with KEGG pathway (top row) and Biological Processes (bottom row) analysis. The bar graph represents significantly enriched annotations of genes with an FDR cutoff of 0.05 and absolute fold change of >2. N., number; ABC, ATP (adenosine 5′-triphosphate)–binding cassette; PPAR, peroxisome proliferator–activated receptor; TNF, tumor necrosis factor; TRP, transient receptor potential.

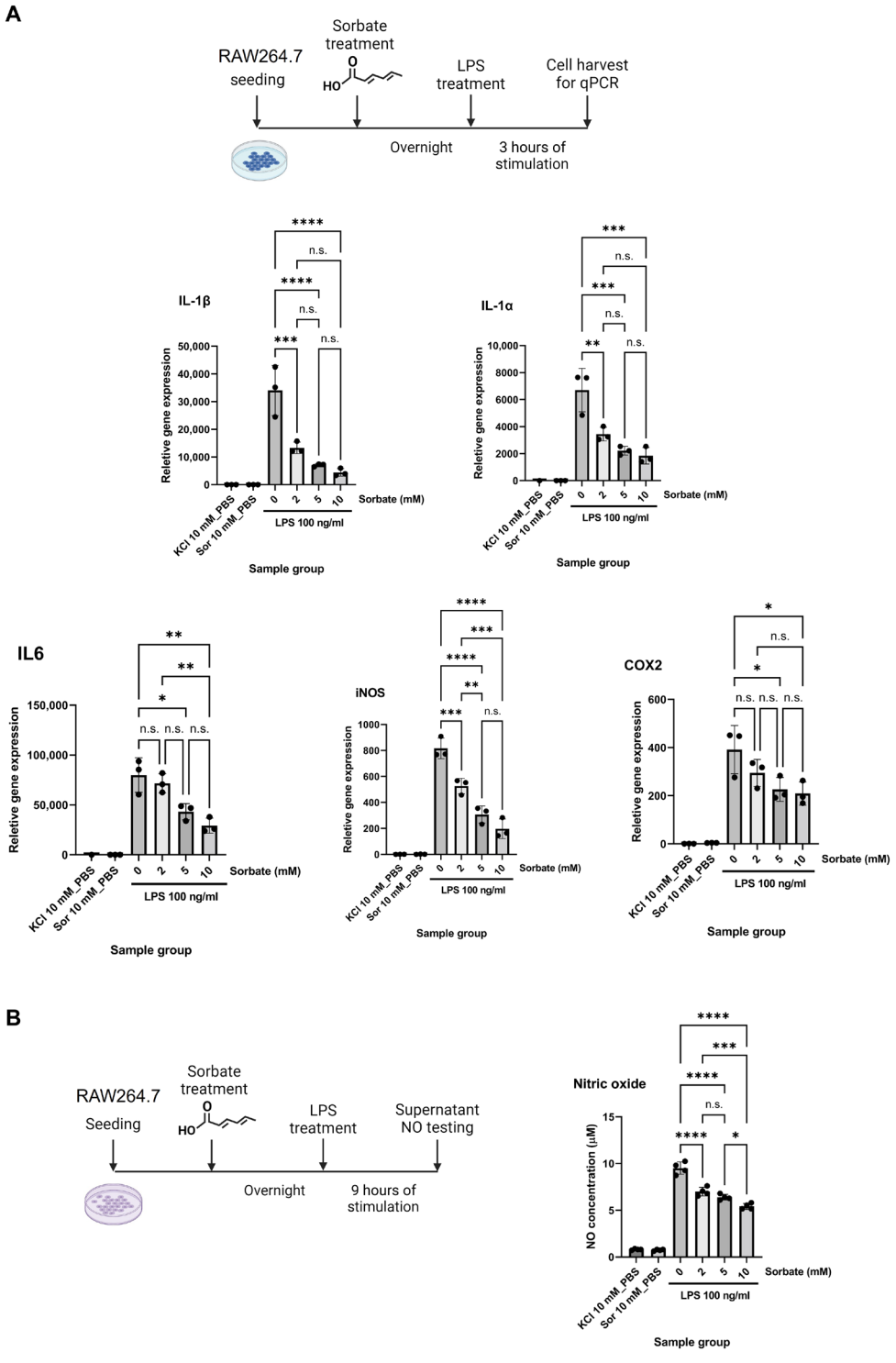

Fig. 5. Sorbate treatment down-regulated inflammation-related gene expression and NO production in RAW 264.7 cells. (**A**) Quantitative polymerase chain reaction (qPCR) analysis of relative expressions of *IL-6*, *IL-1α*, *IL-1β*, *iNOS*, and *COX2* in inflammation response. Cells were treated with various concentrations of potassium sorbate overnight followed by treatment with LPS (100 ng/ml) for 3 hours before cell collection. glyceraldehyde-3-phosphate dehydrogenase was used as an expression control. (**B**) Nitric oxide (NO) assay to evaluate the regulation of nitric oxide production upon sorbate treatment. Cells were treated with various concentrations of potassium sorbate overnight followed by treatment with LPS (100 ng/ml) for 9 hours before cell supernatant collection and nitric oxide assay. Potassium concentration in each assay was maintained by supplementation with potassium chloride. Quantitative analysis one-way ANOVA test with Tukey's multiple comparisons test (biological replicates, $n = 3$ for qPCR analysis and $n = 4$ for NO assays). Error bars represent SD. $^{*}P < 0.05$, $^{**}P < 0.01$, $^{***}P < 0.001$, and $^{****}P < 0.0001$. Created in BioRender (Y. Chen, 2025; https://BioRender.com/f42x375 and https://BioRender.com/d76d802).

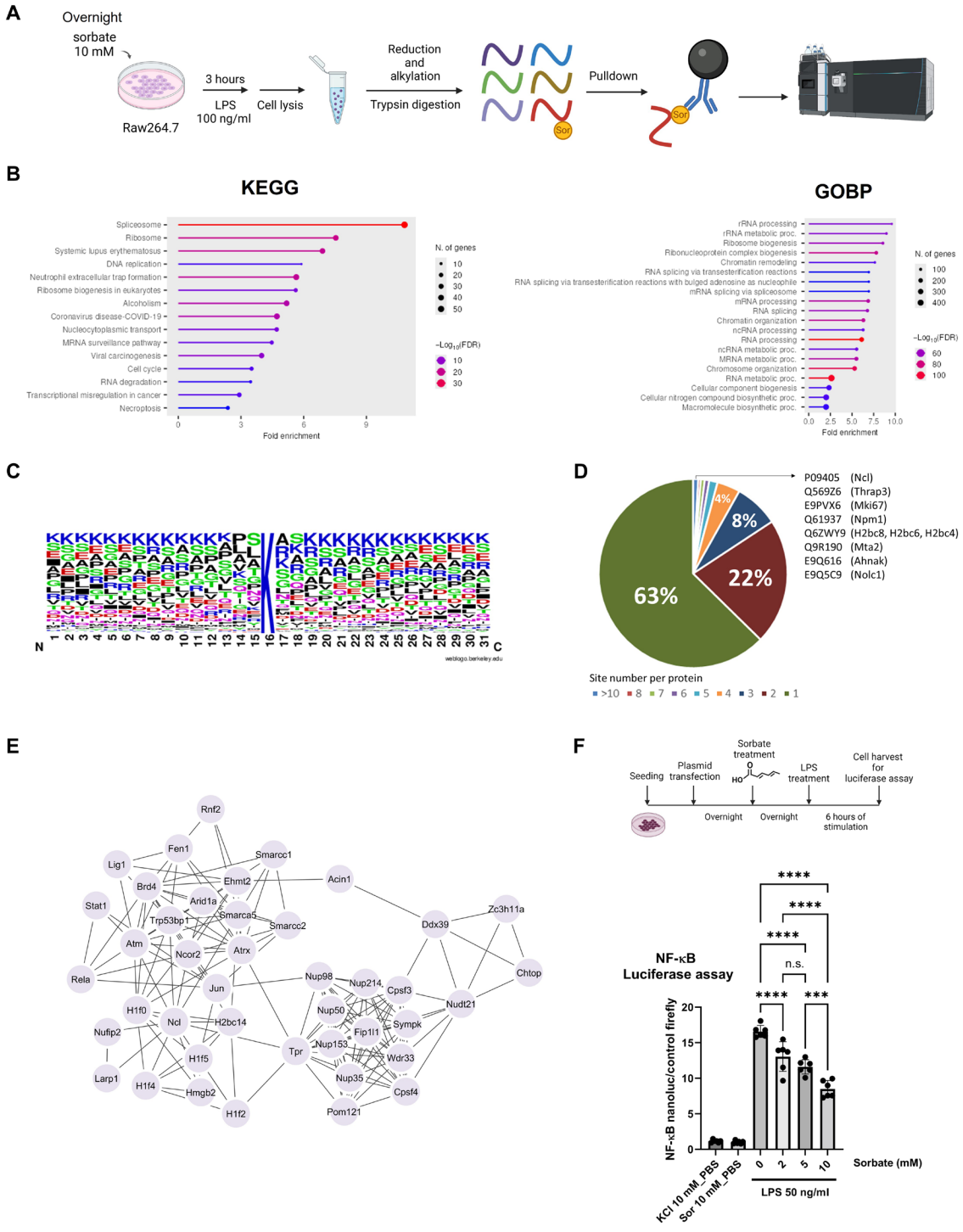

Fig. 6. Global profiling of Ksor substrates and analysis of sorbate-regulation of NF-κB activities. (**A**) Experiment workflow for the immunoprecipitation of lysine sorbylated peptides. Raw264.7 cells were treated with 10 mM sorbate overnight and then stimulated with LPS (100 ng/ml) for 3 hours. Cells were lysed for tryptic digestion. Peptides were immunoprecipitated with pan anti-Ksor antibody and identified by Orbitrap LC-MS analysis. (**B**) Annotation enrichment analysis of Ksor substrates with significantly enriched KEGG pathways and Gene Ontology Biological Processes (GOBP; FDR < 0.05). (**C**) Flanking sequence analysis of Ksor sites with amino acid abundance within ±16 positions. (**D**) Pie chart representing the percentage distribution of site counts in Ksor proteins. (**E**) Network analysis of Ksor proteins identifying a subnetwork with RelA (p65)–interacting proteins. (**F**) Luciferase assay to monitor the effect of sorbate treatment on NF-κB activity. Nanoluc luciferase plasmid with p65 promoter and firefly control plasmid were transfected to Raw264.7 cells, and cells were treated with sorbate for overnight followed by LPS stimulation (50 ng/ml) for 6 hours before cell harvest and luciferase assay. Quantitative analysis one-way ANOVA test with Tukey's multiple comparisons test (biological replicates, $n = 6$). Error bars represent SD. ***$P < 0.001$ and ****$P < 0.0001$, and n.s. indicates not significant ($P > 0.05$). Created in BioRender (Y. Chen, 2025; https://BioRender.com/y38l027 and https://BioRender.com/k20i600).

complex. LC-MS analysis clearly showed that peptides of both histone H3 and p65 could be readily sorbylated in vitro with monosorbylation identified on K4, K9, K14, K18, and K23 on histone H3 and K310, K314, and K315 on p65 (fig. S12).

To determine whether sorbate-induced p65 Ksor correlated with changes in p65 transcriptional activities, we performed luciferase reporter assays in Raw264.7 cells. Upon the transfection of luciferase plasmids, cells were treated with sorbate or vehicle control overnight. Then, cells were stimulated with LPS for 6 hours before harvesting for the luciferase assay (Fig. 6F). Our data showed that cellular uptake of sorbate resulted in a significant and dose-dependent decrease in p65 transcriptional activities corresponding to the increasing concentration of sorbate treatments (Fig. 6F). Together, our global proteomic profiling identified diverse cellular pathways involved in transcription, translation, and inflammation response as Ksor substrates and sorbate treatment dose-dependently reduced p65 transcriptional activity in response to the LPS stimulation.

DISCUSSION

Chemicals in the cellular microenvironment affect physiological activities and organismal functions through diverse mechanisms (*1*–*3*). In this study, we reported that the cellular uptake of sorbate, a widely used food preservative, leads to the chemical modification of lysine side chains on proteins in the form of Ksor. We showed that treatment of mice at a physiological dosage is sufficient to induce sorbylation in the liver. The dynamics of sorbylation are dependent upon sorbate uptake with a relatively quick turnover in several hours (*6*).

Histones were identified and validated as the first Ksor target. Compared to well-characterized histone acetylation and other short-chain acylations such as propionylation and crotonylation, Ksor has a six-carbon chain that is more nonpolar and has a higher hydrophobicity, indicating a potentially larger impact on the properties and protein interactions of histone proteins in nucleosome as well as with other transcription factors (*21*–*23*). A conjugated double bond offers an electron-rich pi-pi interaction potential that may be targeted by previously reported histone readers for lysine crotonylation and benzoylation (*34*–*37*). Such interaction may result in changes in transcriptional activities and gene expression that alter cellular metabolism and signaling. Continued efforts to discover protein binders that mediate the transcriptional activities of histone sorbylation are important to reveal molecular mechanisms of sorbylation-dependent epigenetic changes in physiology and health.

Through investigating sorbylation regulatory enzymes, we identified class I HDACs, including HDAC1, HDAC2, and HDAC3, efficiently remove Ksor and their activities depend on deacetylase activities. Unexpectedly, we found that HDAC1, HDAC2, and HDAC3 can act both as sorbyltransferases when sorbate is present and as desorbylases when sorbate is absent, and its sorbyltransferase activities are dependent upon its deacetylase activity. We demonstrated that HDAC1-3 catalyze such reversible reactions of Ksor in vitro that do not require in situ activation of sorbate through the classic coenzyme A (CoA) activation mechanism (*10*). Our findings do not exclude the possibility that sorbate could be activated into sorbyl-CoA in cells, which may also generate Ksor through the promiscuous activities of histone acetyltransferases (*21*). Identification of class I HDACs as both sorbyltransferases and desorbylases suggests a fast and efficient turnover of lysine acylations from acetylation to sorbylation upon sorbate uptake with an efficient removal of sorbylation in the absence of sorbate. Such reversible catalytic activities of acylation and deacylation are likely not limited to sorbylation and HDAC1-3 enzymes as revealed by recent studies (*33*, *38*), and the types of acylations with corresponding HDAC enzymes remain to be investigated. Furthermore, the catalytic mechanism of how the enzymes mediate the reversible desorbylation and sorbyltransfer reaction is unclear. Studying these mechanisms will offer insights into the cellular dynamics of diverse lysine acylation targets in response to changes in fatty acid and energy metabolism. With HDAC1-3 enzymes as catalytic units of several key corepressor complexes, our findings raise intriguing questions on how activities and epigenetic functions of class I HDAC–related chromatin complexes may be altered upon sorbate uptake and how such changes may affect cellular physiology in human health (*39*).

In our effort to discover the impact of sorbate uptake on gene expression, we performed RNA-seq analysis and discovered that dietary sorbate uptake at a physiological dosage leads to a global down-regulation of inflammation response pathways in mouse liver. Such findings were confirmed in the mouse macrophage Raw267.4 cell model with qPCR measurements of key proinflammatory genes as well as the production of nitric oxide upon LPS stimulation. While acute inflammation is a key defense mechanism to combat pathogens, chronic inflammation is intimately linked with the development and progression of most metabolic and aging-related diseases (*40*). As such, targeting chronic inflammation is a major focus for mitigating disease development (*41*). Given the novel characterization of sorbate regulating inflammatory pathways, the role of sorbate in disease development warrants further investigation.

Through global proteomic analysis, we identified over 900 proteins as Ksor substrates. We revealed that Ksor targets diverse cellular pathways in cells with significant enrichment in translation, RNA processing, and cell signaling. We identified a network of transcription factors and chromatin proteins involved in inflammation response including p65, a key member of the NF-κB complex, Stat1, and Jun as bona fide Ksor targets. As a critical mediator of inflammatory response pathways, activities of the NF-κB complex are essential for the transcription of proinflammatory genes (*40*). Although lysine acetylation is well-known to regulate p65 transcriptional activities, the mechanisms of HDACs in inflammation response are complex (*42*–*44*). It would be intriguing to further study whether sorbylation may cross-talk with acetylation and mediate transcriptional activities in inflammation (*45*–*47*).

The usage of sorbate has markedly increased worldwide in the past decade because of the increasing safety demand for processed food, cosmetic, and pharmaceutical products (*48*). In this study, we found that sorbate uptake efficiently induces Ksor in cells (<5 mM) and mouse tissues (<0.5%) near the level approved by the US Food and Drug Administration, suggesting the physiological relevance of Ksor in regulating organismal metabolism and activities in animal. Our study identified diverse Ksor substrates and determined their potential role in regulating gene expression and signaling with epigenetic histone modifications and transcription factor targets. As various studies link sorbate consumption with cellular abnormalities and potential health risks, further studies are required to determine the role of Ksor in normal physiological development as well as diverse pathological situations such as cancers, metabolic diseases, and aging.

MATERIALS AND METHODS

Materials and reagents

Lipofectamin 3000 (L3000005), Reverse Transcriptase - SuperScript IV VILO Master Mix (11756050), Gibco Dulbecco's modified Eagle medium (DMEM) (11-965-092), Gibco Opti-MEM Reduced Serum Medium (31-985-070), Tris(2-carboxyethyl)phosphine (TCEP)-HCl (PG82080), Laemmli SDS sample buffer (J60015AD), butyrate sodium salt (263191000), and Coomassie Protein Assay Reagent (PI23236) were from Thermo Fisher Scientific (Waltham, MA). Sorbic acid (S1626-100G), potassium sorbate (85520-50G), Luminata Crescendo horseradish peroxidase (HRP) substrates (WBLUR0500), Roche cOmplete protease inhibitor cocktail tablet (04693116001), *N*-1-naphthylethylenediamine dihydrochloride (222488), nicotinamide (N3376), sulfanilamide (S9251), fetal bovine serum (F0926), LPS (L4391), Amicon filter (Ultra-15), MISSION siRNA Universal Negative Control (sic001), and siRNAs targeting HDAC1 (SASI_Hs01_00079968) and HDAC2 (SASI_Hs01_00142115) were from Millipore-Sigma (St. Louis, MO). siRNA targeting HDAC3 (hs.Ri.HDAC3.13.1) was from Integrated DNA Technologies (Coralville, IA). Recombinant HDAC1 (50051), HDAC2 (50002), and HDAC3/NCOR2 (50003) were from BPS Bioscience (San Diego, CA). Sorbic acid–$^{13}C_2$ (S676891) was from Toronto Research Chemicals (Toronto, Ontario, Canada). TSA was from MedchemExpress (Monmouth Junction, NJ). Iodoacetamide (IAA) (02327) was from Chem-Impex (Wood Dale, IL). DharmaFECT 1 Transfection Reagent was from Horizon Discovery (Cambridge, UK). The Monarch Total RNA Miniprep Kit (T1020S) and Luna Universal qPCR Master Mix (M3003) were from New England Biolabs (Ipswich, MA). An RNeasy RNA mini kit (74104) was from QIAGEN (Venlo, The Netherlands). Trypsin (V5280), Nano-Glo Dual Luciferase Reporter (NanoDLR) Assay System with One Glo Reagent and Stop&Glo Reagent (N1610), and luciferase assay plasmids (pNL3.2.NF-κB-RE[NlucP/NF-κB-RE/Hygro] and pGL4.54[luc2/TK]) were from Promega (Madison, WI). Penicillin and streptomycin solution (100×; 25-512) was from Genesee Scientific (Morrisville, NC). HiTrap protein A resin (17040203) and rProtein A GraviTrap (28-9852-54) were from Cytiva Life Sciences (Marlborough, MA). Empore C18 membrane was from CDS Analytical (Oxford, PA). The Mycoplasma PCR Detection Kit (G238) was from Applied Biological Materials (Richmond, British Columbia, Canada). Anti-rabbit immunoglobulin G (IgG) HRP-linked antibody (7074S), anti-mouse IgG HRP-linked antibody (7076S), pan anti-acetylated lysine antibody (9441), anti-acetylated-lysine (Ac-K2-100) MultiMab Rabbit mAb mix (9814), and β-actin (8H10D10) were from Cell Signaling (Danvers, MA). Anti-HDAC1 (815102), HDAC2 (680101), and HDAC3 (685201) antibodies were from BioLegend (San Diego, CA). HDAC inhibitors MS275 (Entinostat, HY-12163) and TSA (HY-15144) were from MedChemExpress (Monmouth Junction, NJ). SIS17 (S6687), UF010 (S5810), and TMP195 (S8502) were from Selleckchem (Houston, TX). Zinc sulfate [B4382-01, American Chemical Society (ACS) grade] was from Avantor Performance Materials (Radnor, PA).

Cell culture

Cells were maintained at 37°C and 5% CO_2 in DMEM, supplemented with 10% fetal bovine serum, 100 IU of penicillin, and streptomycin (100 μg/ml). 293T (CRL-3216), RAW 264.7 (TIB-71), HepG2 (HB-8065), and HCT116 (CCL-247) were from American Type Cell Culture (Manassas, Virginia). Mycoplasma was routinely monitored by the Mycoplasma PCR Detection Kit in inflammation and HDAC-related cell experiments.

Histone extraction

Cells were scraped down by PBS with 20 mM nicotinamide and 10 mM sodium butyrate. Then, the cell pellets were spun down and lysed by PBS with 0.5% Triton X-100, 1× cOmplete protease inhibitor, 40 mM nicotinamide, and 20 mM sodium butyrate. The nuclear was further spun down and extracted by 0.4 N H_2SO_4 overnight at 4°C. Then, proteins were precipitated by 20% (v/v) trichloroacetic acid, and the precipitated pellet was further washed with ice-cold acetone. To enable SDS gel analysis, the extract was dissolved by nonreducing sample buffer [2% SDS, 10% glycerol, 0.002% bromophenol blue, and 100 mM tris-Cl (pH 6.8)].

Histone in-gel digestion

After the gel was destained, the histone bands were cut, washed thoroughly with water, and incubated with 50% ethanol at room temperature with rotation for 1 hour. The gel was further washed with water, cut into pieces, and washed with 50% acetonitrile and 100% acetonitrile. Then, the gel pieces were dried down by SpeedVac (Thermo Fisher Scientific, Waltham, MA). The dried gel pieces were rehydrated with trypsin buffer (1 μg/100 μl of 100 mM ammonium bicarbonate) and incubated at 37°C overnight. The digestion solution was first transferred, and the peptides in gel pieces were then extracted by 50% acetonitrile and 100% acetonitrile sequentially. Last, all the peptide solutions were pulled together and dried by SpeedVac and desalted using in-house packed C18 StageTip for LC-MS analysis.

Development of pan anti-Ksor antibody

Pan anti-Ksor antibody was developed and purified with the following procedures as previously described (*23, 49, 50*). Briefly, lysine-sorbylated keyhole limpet hemocyanin was applied to immunize rabbits, and serum titer was monitored by enzyme-linked immunosorbent assay (Genemed Synthesis, San Antonio, TX). Pan anti-Ksor antibody was purified from serum using sorbyllysine-conjugated agarose beads and eluted with 0.1 M glycine-HCl (pH 2.5), followed by immediate neutralization with 1 M tris-HCl (pH 8.9). The antibody was further dialyzed and concentrated in 1× PBS with an Amicon filter.

Western blotting

To analyze the whole proteome lysate through Western blot, cells were washed with 1× PBS and lysed by Laemmli SDS sample buffer. Then, the lysate was boiled briefly at 99°C with shaking at 800 rpm. Last, the samples were resolved on SDS–polyacrylamide gel electrophoresis (PAGE), and proteins were transferred to the polyvinylidene difluoride membrane. The membrane was blocked by 5% skim milk or bovine serum albumin (BSA) in PBS with 0.1% Tween 20. The membrane was further incubated with primary antibody and HRP-conjugated secondary antibody. Last, the membrane was developed with Luminata Crescendo Western HRP Substrate for signal detection.

Dot blot assay

Peptide solutions at various concentrations were dotted onto the nitrocellulose membrane. After the peptide dots were dried, the membrane was blocked with BSA in 1× PBS with 0.1% Tween 20. Then, the membrane was subjected to incubation with primary and HRP-linked secondary antibodies. Signals were developed with Luminata Crescendo HRP substrates.

Isotopic labeling of Ksor

HCT116 cells were treated with 2 mM [$^{13}C_2$]sorbic acid for 24 hours. After the treatment, histones were extracted for SDS-PAGE, stained with Coomassie blue staining, and in-gel tryptic digested. The extracted peptides were desalted followed by LC-MS analysis.

HPLC co-elution with synthetic peptides

Sorbylated peptides were synthesized and purified by GL Biochem Ltd. (Shanghai, China) with Fmoc-sorbyllysine (WuXi AppTec, Shanghai, China). The concentration of synthetic peptide solutions was adjusted approximately to match the MS intensities of endogenous sorbylated histone peptides. Endogenous histone peptides, synthetic peptides, and their equal mixtures were analyzed through the same HPLC gradient in LC-MS analysis with thorough washes in between. Extracted ion chromatograms of mass spectrometry data based on the mass-to-charge ratios of targeted peptides were presented.

Assay of nitric oxide production in RAW264.7

RAW264.7 cells were seeded in 24-well plates overnight. Then, the cells were treated with sorbate for 15 hours. After the sorbate treatment, LPS was given to cells for the other 9 hours of incubation. Supernatant (100 μl) from the cell was tested by mixing with 50 μl of 0.1% *N*-1-naphthylethylenediamine dihydrochloride in water and 50 μl of 1% sulfanilamide in 5% phosphoric acid. Sodium nitrite dissolved in water was used as standard curve construction. Last, the product was detected by absorption spectroscopy at 545 nm.

HDAC knockdown

293T cells were seeded in 12-well plates. siRNA (0.05 nmol each) targeting human HDAC1, HDAC2, or HDAC3 was mixed with DharmaFECT 1 transfection reagent with DMEM and incubated with cells for 30 hours, while the control cells with sorbate treatment were added with siRNA Universal Negative Control (0.05 nmol) mixed with DharmaFECT 1 transfection reagent in DMEM, and the control cells without sorbate treatment were added only with DharmaFECT 1 transfection reagent in DMEM. After the incubation, the original medium was replaced with fresh DMEM and subjected to treatments with sorbate or PBS.

HDAC in vitro assay

Desorbylase activity assay

Histones extracted from 293T cells treated with 10 mM sorbic acid for 24 hours were reconstituted by the assay buffer [PBS with 1 mM $MgCl_2$, 10 μM zinc sulfate, and 10 mM tris (pH 7.5 to 8.5)] to a final concentration of 0.5 mg/ml. Then, histones were incubated with an HDAC enzyme at a final concentration of 500 nM with or without 40 mM butyrate for incubation with rotation at 37°C for 24 hours. Last, reactions were stopped by boiling in a nonreducing sampling buffer [2% SDS, 10% glycerol, 0.002% bromophenol blue, and 100 mM tris-Cl (pH 6.8)] for Western blot and Coomassie blue staining analysis.

Sorbyltransferase activity assay with extracted histones

Histones extracted from regular 293T cells were reconstituted in the assay buffer as above to a final concentration of 0.5 mg/ml. Then, histones were incubated with an HDAC enzyme at a final concentration of 500 nM with or without various concentrations of potassium sorbate or TSA (50 μM) for incubation with rotation at 37°C for 24 hours. Last, reactions were stopped by boiling in the nonreducing sampling buffer for Western blot and Coomassie blue staining analysis.

Sorbyltransferase activity assay with synthetic peptides

The mixture of the following peptides at a concentration of 25 μM each was suspended in the reaction buffer [PBS with 1 mM $MgCl_2$, 10 μM zinc sulfate, and 10 mM tris (pH 7.5 to 8.5)] and incubated with or without sorbate (20 mM) and HDAC enzyme (500 nM) for 18 hours at 37°C. Then, the reaction was quenched by 0.1% Trifluoroacetic acid (TFA) and desalted for LC-MS analysis. The fragment ion analysis was performed using Molecular Weight Calculator from the Pacific Northwest National Laboratory (PNNL).

Ac-H3(3-16): Ac-TKQTARKSTGGKAP-$CONH_2$
H3(13-26): NH_2-GGKAPRKQLATKAA-$CONH_2$
H4(2-18): NH_2-SGRGKGGKGLGKGGAKR-$CONH_2$
p65(305-320): NH_2-TYETFKSIMKKSPFSG-$CONH_2$

Immunoprecipitation of Ksor peptides

Raw264.7 cells were seeded in 15-cm plates and treated with 10 mM potassium sorbate overnight. Then, the cells were stimulated by LPS at 100 ng/ml for 3 hours. The treated cells were scraped down in PBS and lysed in denaturing lysis buffer (9 M urea with 1× cOmplete protease inhibitor), followed by reduction and alkylation with TCEP and IAA at the final concentration of 10 mM at room temperature in dark. Then, the reaction was quenched by cysteine (20 mM). The cell lysate was diluted to 1.5 M urea with 100 mM ammonium bicarbonate, and trypsin was added at an enzyme-to-substrate ratio of 1:50 (w/w) for proteolytic digestion at 37°C overnight. The digested peptides were desalted and dried in SpeedVac (Thermo Fisher Scientific, Waltham, MA). The dried peptides were dissolved in the immunoprecipitation (IP) buffer (1× PBS with 0.1% Tween 20) and incubated with protein A beads pre-conjugated with pan anti-sorbylation antibody overnight. The beads were washed with the IP buffer four times and 1× PBS four times. Last, the peptides were eluted by 0.1% TFA three times. The eluted peptides were desalted using in-house packed C18 StageTip for LC-MS analysis.

Conversion of sorbate ADI between human and mouse

ADI of sorbate for man is 25 mg/kg of body weight (*27*). Based on the formula below (*28*)

$$\text{Animal equivalent dose}\,(\text{mg/kg}) = \text{Human dose}\,(\text{mg/kg})/\text{Km ratio}$$

(Km ratio is the correction factor, and the value is 0.081 to convert the human dose to the mouse dose.)

From this calculation, we obtained the sorbate ADI for mice as 308.6 mg/kg. If we assume that the reference body weight of mouse is 25 g or 0.025 kg (*51*), then we obtained the equivalent dose of sorbate uptake per day as 7.7 mg. If we assume that mice eat 4 g of food per day, then the percentage of sorbate in food in mouse diet is ~0.2%.

Treatment of mice with a diet containing potassium sorbate via oral gavage

Twelve mice (C57BL6/J males ~ 10 weeks of age) were given either a control (water) bolus ($n = 4$) or 17 mg of potassium sorbate via oral gavage. This dosage represents the approximate average daily intake of potassium sorbate around 0.5% of the diet during the feeding trial. The control mice were euthanized immediately, and sorbate mice were euthanized 2 or 4 hours after gavage ($n = 4$ per group). Mice-related

experiments in this study were approved by the Institutional Animal Care and Use Committee at the University of Minnesota Twin Cities.

Mouse liver RNA extraction and sequencing

RNA was extracted from snap-frozen liver tissue using the RNeasy RNA mini kit. Eukaryotic RNA isolates were quantified using a fluorometric RiboGreen assay. The total RNA integrity was assessed using capillary electrophoresis. Only samples higher than 1 μg with an RNA integrity number (RIN) of 8 or greater proceeded to sequencing. Total RNA samples were converted to Illumina sequencing libraries using Illumina's TruSeq RNA sample preparation kit. One microgram of total RNA was oligo(dT) purified using oligo(dT)-coated magnetic beads, fragmented, and then reverse transcribed into cDNA. The cDNA was fragmented, blunt-ended, and ligated to indexed (barcoded) adaptors and amplified using 15 cycles of PCR. The final library size distribution was validated using capillary electrophoresis and quantified using fluorimetry (Pico Green) and via qPCR. Indexed libraries were then normalized, pooled, and size selected to 320 base pairs (bp) using a Caliper XT instrument. TruSeq libraries were hybridized to a single read flow cell, and individual fragments were clonally amplified by bridge amplification on the Illumina cBot. Once complete, the flow cell was loaded on the Hi-Seq 2500 and sequenced. Upon completion of read 1, an 8-bp forward and 8-bp reverse (i7 and i5) index read was performed. Base call files for each cycle of sequencing were generated by Illumina Real-Time Analysis software. Primary analysis and demultiplexing were performed using Illumina bcl2fatstq software version 2.17.1.14.

Data alignment and gene quantification were analyzed using the CHURP pipeline at the University of Minnesota Supercomputing Institute. FASTQ paired-end reads (2 × 150 bp) for 12 samples (26.1 million reads average per sample) were trimmed using Trimmomatic (v0.33) enabled with the optional "-q" option; 3-bp sliding-window trimming from 3′ end requiring minimum Q30. Quality control on raw sequence data for each sample was performed with FastQC. Read mapping was performed via HISAT2 (v2.1.0) (*52*) using the mouse genome (GRCm38) as a reference. Gene quantification was done via Feature Counts for raw read counts. DEGs were analyzed by R with the edgeR library using raw read count as input. The volcano plot and heatmap figures were generated with the libraries including ggplot2, ggrepel, pheatmap, dplyr, and annotables. We filtered the generated list on the basis of a minimum absolute fold change > 2 and adjusted FDR < 0.05.

qPCR assay

RAW264.7 cells were treated with various concentrations of potassium sorbate overnight followed by LPS at 100 ng/ml for 3 hours before harvesting. The total RNA was extracted by the Monarch Total RNA Miniprep Kit and subjected to reverse transcription with SuperScript IV VILO Master Mix according to the manufacturer's instructions. Last, qPCR was performed with Luna Universal qPCR Master Mix and the primers below. Gene expression values of IL-6 and IL-1α with levels below the detection limit in cells without LPS stimulation were deleted in qPCR analysis.

1. Mouse *GAPDH* primers: forward sequence, CATCACTGCCACCCAGAAGACTG; and reverse sequence, ATGCCAGTGAGCTTCCCGTTCAG

2. Mouse *IL-6* primers: forward sequence, TACCACTTCACAAGTCGGAGGC; and reverse sequence, CTGCAAGTGCATCATCGTTGTTC

3. Mouse *PTGS2* (Prostaglandin G/H synthase 2) (Cox2) primers: forward sequence, GCGACATACTCAAGCAGGAGCA; and reverse sequence, AGTGGTAACCGCTCAGGTGTTG

4. Mouse *iNOS2* primers: forward sequence, GAGACAGGGAAGTCTGAAGCAC; and reverse sequence, CCAGCAGTAGTTGCTCCTCTTC

5. Mouse *IL-1*α primers: forward sequence, CGAAGACTACAGTTCTGCCATT; and reverse sequence, GACGTTTCAGAGGTTCTCAGAG

6. Mouse *IL-1*β primers: forward sequence, GCCACCTTTTGACAGTGATGAG; and reverse sequence, GACAGCCCAGGTCAAAGGTT

LC-MS analysis

Peptides were analyzed with the Dionex Ultimate 3000 RSLC nano HPLC system with an Orbitrap Fusion Lumos Tribrid Mass Spectrometer (Thermo Fisher Scientific, Waltham, MA) similarly as previously described (*53*). Briefly, digested peptides dissolved in HPLC buffer A [0.1% formic acid in water (v/v)] were separated on an in-house packed capillary HPLC column (length of 20 cm and inner diameter of 75 μm) from CoAnn Technologies (Richland, WA) with Luna C18 beads (particle size of 5 μm and pores of 100 Å) from Phenomenex (Torrance, CA). The peptides were separated with a gradient from 1 to 95% HPLC buffer B [0.1% formic acid in acetonitrile (v/v)] in HPLC buffer A. Full scan of precursor ions (MS1) was performed in a positive mode in Orbitrap, and MS/MS analysis was performed in the linear ion trap with a 35% of normalized high-energy collision dissociation energy.

Luciferase assay

Raw 264.7 cells were seeded in 12-well plates overnight and then transfected with NF-κB Nanoluc plasmid and control Firefly plasmid with Lipofectamine 3000 on the basis of the manufacturer's protocol. After overnight transfection, medium was replaced with fresh DMEM, and cells were treated with various concentrations of potassium sorbate or potassium chloride overnight. Then, cells were treated with LPS for 6 hours. After the LPS stimulation, medium was removed, and cells were briefly rinsed with PBS followed by lysis with passive lysis buffer. The protein lysate was centrifuged at 21,000*g* for 5 min at 4°C to remove pellets. ONE Glo Reagent was added to the supernatant of the lysate to measure firefly luminescence, and Stop&Glo reagent was added to measure the second luminescence.

Database searching

LC-MS data were analyzed with the MaxQuant database search engine (version 2.2.0.0) (*54*). UniProt mouse protein database (UP000000589_10090) was searched for the LC-MS analysis of Ksor immunoprecipitation from Raw264.7 cells. A small database containing human and mouse histone proteins from the UniProt protein database was searched for the LC-MS analysis of extracted histones. Trypsin was specified as the protease, and the maximum number of missing cleavages was set as 4. Cysteine carbamidomethylation was set as a fixed modification for Ksor immunoprecipitation sample analysis. Methionine oxidation, protein N-terminal acetylation, lysine acetylation, and Ksor were defined as variable modifications. Sorbylation modification was defined as C(6)H(6)O and neural loss was set as C(6)H(6)O. Lysine sorbylation and acetylation were not allowed on peptide C-termini. The maximum number of modifications per peptide was set as 4.

Quantification of histone epigenetic marks with EpiProfile analysis

293T cells were treated by 10 mM potassium sorbate or PBS for about 24 hours. The histones were extracted as described above. The extracted histone was derivatized with propionic anhydride and then digested by trypsin following the previously described procedure by the Garcia lab (*29*).

Histone peptides were analyzed with data-independent analysis by Orbitrap nanoLC-MS/MS following the previously described setup including central mass/charge ratio, isolation window, and scan range (*29*). MS2 activation type was set as collision-induced dissociation (CID) with the collision energy set at 30%. Quadrupole isolation was enabled in both MS1 and MS2.

Histone mass spectra data were processed using EpiProfile 2.1 (*55*). Briefly, human histone sequences underwent in silico digestion into peptides, with cleavage occurring after arginine. Each peptide was then assessed for potential PTMs, such as H3 3-8 unmodified, K4me1, K4me2, K4me3, and K4ac. The area under the curve (AUC) for each peptide was extracted from the raw data. To normalize and facilitate group comparisons, the percentage of each peptide within the same sequence was calculated by dividing its AUC by the summed AUC. The program is available for downloading at GitHub (https://github.com/zfyuan/EpiProfile2.0_Family/blob/master/EpiProfile2.1_basic_Ksor.zip).

Peptide synthesis

Peptides were synthesized using standard Fmoc chemistry on Rink amide resin (0.05 mmol, Gyros Protein Technologies) with a Symphony X automated peptide synthesizer (Gyros Protein Technologies). Fmoc deprotection was performed in 20% piperidine (two times for 5 min), and peptide elongation was carried out by coupling Fmoc-protected amino acids (6 equiv, Gyros Protein Technologies) applying HCTU [O-(1H-6-Chlorobenzotriazole-1-yl)-1,1,3,3-tetramethyluronium hexafluorophosphate] (5.7 equiv, Gyros Protein Technologies) and NMM (N′-Methyl morpholine) (12 equiv, Thermo Scientific) for activation (two times for 20 min). Peptides were cleaved from resin, and their sidechains were deprotected in a cocktail of 94% trifluoroacetic acid (Sigma-Aldrich), 2.5% water, 2.5% ethanedithiol (Sigma-Aldrich), and 1% triisopropylsilane (ChemImpex). Following cleavage, peptides were precipitated and washed thrice with ice-cold diethyl ether (Thermo Fisher Scientific) before redissolving the final peptide pellet with aqueous acetonitrile and freeze drying.

Peptides were purified via RP-LC-MS using an Agilent 1200 Series HPLC on an Agilent Zorbax 300SB-C18 column (5 μm, 9.4 mm by 250 mm) at flow rate of 4 ml/min. Eluted peptides were identified with an Agilent 6130A mass spectrometer. Before application, p65(305-320) was analyzed via RP-LC-MS using an Agilent 1200 Series HPLC connected to an Agilent 6130A MS on an Sepax Bio-C18 column (5 μm, 2.1 mm by 50 mm) with a flow rate of 0.5 ml/min using a gradient of aqueous acetonitrile (with 0.1% formic acid) increasing from 0% acetonitrile at 5 min to 40% at 12 min. Peptides H3 (*13*–*26*) and H4 (*2*–*14*) were analyzed using an aqueous acetonitrile gradient of 0–30% from 10 to 30 min on a (Agilent Zorbax 300SB-C18, 5 μm, 2.1 mm by 250 mm). Peptide Ac-H3 (*3*–*16*) was analyzed using an aqueous acetonitrile gradient of 0 to 8% from 10 to 30 min on a (Agilent Zorbax 300SB-C18, 5 μm, 2.1 mm by 250 mm).

Bioinformatics

For protein cluster interaction analysis, Ksor protein interaction network was extracted from the STRING database with default criteria and exported for presentation with Cytoscape (*56*, *57*). Subnetworks of Ksor protein clusters were identified with MCODE analysis (*58*). Annotation enrichment analysis of DEGs for Kyoto Encyclopedia of Genes and Genomes (KEGG) pathway and Gene Ontology Biological Processes was done using ShinyGo (version 0.81, FDR < 0.05) (*59*). Flanking sequence analysis was performed with Weblogo (version 3) with ±16 positions of Ksor sites (*60*). Additional R packages were used for programing including readxl, dplyr, and openxlsx. GraphPad prism (GraphPad Software, Boston, MA) was used for bar graph representation with statistical analysis. Figure preparation was assisted by BioRender. Chemical structures were drawn with ChemSketch 2022.2.2 version.

Supplementary Materials

The PDF file includes:

Figs. S1 to S12

Legends for data S1 to S4

Other Supplementary Material for this manuscript includes the following:

Data S1 to S4

REFERENCES AND NOTES

1. B. R. Sabari, D. Zhang, C. D. Allis, Y. Zhao, Metabolic regulation of gene expression through histone acylations. *Nat. Rev. Mol. Cell Biol.* **18**, 90–101 (2017).
2. A. Baccarelli, V. Bollati, Epigenetics and environmental chemicals. *Curr. Opin. Pediatr.* **21**, 243–251 (2009).
3. C. Tiffon, The impact of nutrition and environmental epigenetics on human health and disease. *Int. J. Mol. Sci.* **19**, 3425 (2018).
4. H. Huang, D. Zhang, Y. Wang, M. Perez-Neut, Z. Han, Y. G. Zheng, Q. Hao, Y. Zhao, Lysine benzoylation is a histone mark regulated by SIRT2. *Nat. Commun.* **9**, 3374 (2018).
5. "Evaluation of the health aspects of sorbic acid and its salts as food ingredients" (PB262663, Federation of American Societies for Experimental Biology; Life Sciences Research Office; Food and Drug Administration, Bureau of Foods, 1975); https://ntrl.ntis.gov/NTRL/dashboard/searchResults/titleDetail/PB262663.xhtml.
6. R. Walker, Toxicology of sorbic acid and sorbates. *Food Addit. Contam.* **7**, 671–676 (1990).
7. 4: Final report on the safety assessment of sorbic acid and potassium sorbate. *J. Am. Coll. Toxicol.* **7**, 837–880 (1988).
8. EFSA Panel on Food Additives and Nutrient Sources added to Food (ANS), Scientific Opinion on the re-evaluation of sorbic acid (E 200), potassium sorbate (E 202) and calcium sorbate (E 203) as food additives. *EFSA J.* **13**, 4144 (2015).
9. A. Bajcic, R. B. Petronijevic, M. Sefer, D. Trbovic, V. Djordjevic, J. Ciric, A. Nikolic, Sorbates and benzoates in meat and meat products: Importance, application and determination. *IOP Conf. Ser. Earth Environ. Sci.* **854**, 012005 (2021).
10. P. Dehghan, A. Mohammadi, H. Mohammadzadeh-Aghdash, J. E. N. Dolatabadi, Pharmacokinetic and toxicological aspects of potassium sorbate food additive and its constituents. *Trends Food Sci. Technol.* **80**, 123–130 (2018).
11. S. Mamur, D. Yüzbaşıoğlu, F. Ünal, S. Yılmaz, Does potassium sorbate induce genotoxic or mutagenic effects in lymphocytes? *Toxicol. In Vitro* **24**, 790–794 (2010).
12. Z.-F. Luo, X.-L. Fang, G. Shu, S.-B. Wang, X.-T. Zhu, P. Gao, L.-L. Chen, C.-Y. Chen, Q.-Y. Xi, Y.-L. Zhang, Q.-Y. Jiang, Sorbic acid improves growth performance and regulates insulin-like growth factor system gene expression in swine. *J. Anim. Sci.* **89**, 2356–2364 (2011).
13. E. A. Yu, J. O. Alemán, D. R. Hoover, Q. Shi, M. Verano, K. Anastos, P. C. Tien, A. Sharma, A. Kardashian, M. H. Cohen, E. T. Golub, K. G. Michel, D. R. Gustafson, M. J. Glesby, Plasma metabolomic analysis indicates flavonoids and sorbic acid are associated with incident diabetes: A nested case-control study among Women's Interagency HIV Study participants. *PLOS ONE* **17**, e0271207 (2022).
14. B. Raposa, R. Pónusz, G. Gerencsér, F. Budán, Z. Gyöngyi, A. Tibold, D. Hegyi, I. Kiss, Á. Koller, T. Varjas, Food additives: Sodium benzoate, potassium sorbate, azorubine, and tartrazine modify the expression of NFκB, GADD45α, and MAPK8 genes. *Physiol. Int.* **103**, 334–343 (2016).
15. C.-H. Chen, S.-N. Ho, P.-A. Hu, Y. R. Kou, T.-S. Lee, Food preservative sorbic acid deregulates hepatic fatty acid metabolism. *J. Food Drug Anal.* **28**, 206–216 (2020).

16. C. T. Walsh, S. Garneau-Tsodikova, G. J. Gatto Jr., Protein Posttranslational Modifications: The chemistry of proteome diversifications. *Angew. Chem. Int. Ed. Engl.* **44**, 7342–7372 (2005).
17. H. Lin, K. T. Caroll, Introduction: Posttranslational protein modification. *Chem. Rev.* **118**, 887–888 (2018).
18. G. Figlia, P. Willnow, A. A. Teleman, Metabolites regulate cell signaling and growth via covalent modification of proteins. *Dev. Cell* **54**, 156–170 (2020).
19. E. K. Keenan, D. K. Zachman, M. D. Hirschey, Discovering the landscape of protein modifications. *Mol. Cell* **81**, 1868–1878 (2021).
20. Y. Zhao, B. A. Garcia, Comprehensive catalog of currently documented histone modifications. *Cold Spring Harb. Perspect. Biol.* **7**, a025064 (2015).
21. Y. Chen, R. Sprung, Y. Tang, H. Ball, B. Sangras, S. C. Kim, J. R. Falck, J. Peng, W. Gu, Y. Zhao, Lysine propionylation and butyrylation are novel post-translational modifications in histones. *Mol. Cell. Proteomics* **6**, 812–819 (2007).
22. Z. Zhang, M. Tan, Z. Xie, L. Dai, Y. Chen, Y. Zhao, Identification of lysine succinylation as a new post-translational modification. *Nat. Chem. Biol.* **7**, 58–63 (2011).
23. M. Tan, H. Luo, S. Lee, F. Jin, J. S. Yang, E. Montellier, T. Buchou, Z. Cheng, S. Rousseaux, N. Rajagopal, Z. Lu, Z. Ye, Q. Zhu, J. Wysocka, Y. Ye, S. Khochbin, B. Ren, Y. Zhao, Identification of 67 histone marks and histone lysine crotonylation as a new type of histone modification. *Cell* **146**, 1016–1028 (2011).
24. D. Zhang, Z. Tang, H. Huang, G. Zhou, C. Cui, Y. Weng, W. Liu, S. Kim, S. Lee, M. Perez-Neut, J. Ding, D. Czyz, R. Hu, Z. Ye, M. He, Y. G. Zheng, H. A. Shuman, L. Dai, B. Ren, R. G. Roeder, L. Becker, Y. Zhao, Metabolic regulation of gene expression by histone lactylation. *Nature* **574**, 575–580 (2019).
25. Z. Xie, D. Zhang, D. Chung, Z. Tang, H. Huang, L. Dai, S. Qi, J. Li, G. Colak, Y. Chen, C. Xia, C. Peng, H. Ruan, M. Kirkey, D. Wang, L. M. Jensen, O. K. Kwon, S. Lee, S. D. Pletcher, M. Tan, D. B. Lombard, K. P. White, H. Zhao, J. Li, R. G. Roeder, X. Yang, Y. Zhao, Metabolic regulation of gene expression by histone lysine β-hydroxybutyrylation. *Mol. Cell* **62**, 194–206 (2016).
26. C. Peng, Z. Lu, Z. Xie, Z. Cheng, Y. Chen, M. Tan, H. Luo, Y. Zhang, W. He, K. Yang, B. M. M. Zwaans, D. Tishkoff, L. Ho, D. Lombard, T.-C. He, J. Dai, E. Verdin, Y. Ye, Y. Zhao, The first identification of lysine malonylation substrates and its regulatory enzyme. *Mol. Cell. Proteomics* **10**, M111.012658 (2011).
27. "274. Sorbic acid and its calcium, potassium and sodium salts" (WHO Food Additives Series 5, 1974); www.inchem.org/documents/jecfa/jecmono/v05je18.htm.
28. A. B. Nair, S. Jacob, A simple practice guide for dose conversion between animals and human. *J Basic Clin Pharm.* **7**, 27–31 (2016).
29. K. R. Karch, S. Sidoli, B. A. Garcia, Identification and quantification of histone PTMs using high-resolution mass spectrometry. *Methods Enzymol.* **574**, 3–29 (2016).
30. C. Moreno-Yruela, D. Zhang, W. Wei, M. Bæk, W. Liu, J. Gao, D. Danková, A. L. Nielsen, J. E. Bolding, L. Yang, S. T. Jameson, J. Wong, C. A. Olsen, Y. Zhao, Class I histone deacetylases (HDAC1–3) are histone lysine delactylases. *Sci. Adv.* **8**, eabi6696 (2022).
31. W. Wei, X. Liu, J. Chen, S. Gao, L. Lu, H. Zhang, G. Ding, Z. Wang, Z. Chen, T. Shi, J. Li, J. Yu, J. Wong, Class I histone deacetylases are major histone decrotonylases: Evidence for critical and broad function of histone crotonylation in transcription. *Cell Res.* **27**, 898–915 (2017).
32. P. M. Lombardi, K. E. Cole, D. P. Dowling, D. W. Christianson, Structure, mechanism, and inhibition of histone deacetylases and related metalloenzymes. *Curr. Opin. Struct. Biol.* **21**, 735–743 (2011).
33. S. Sun, Z. Xu, L. He, Y. Shen, Y. Yan, X. Lv, X. Zhu, W. Li, W.-Y. Tian, Y. Zheng, S. Lin, Y. Sun, L. Li, Metabolic regulation of cytoskeleton functions by HDAC6-catalyzed α-tubulin lactylation. *Nat. Commun.* **15**, 8377 (2024).
34. Y. Li, B. R. Sabari, T. Panchenko, H. Wen, D. Zhao, H. Guan, L. Wan, H. Huang, Z. Tang, Y. Zhao, R. G. Roeder, X. Shi, C. D. Allis, H. Li, Molecular coupling of histone crotonylation and active transcription by AF9 YEATS domain. *Mol. Cell* **62**, 181–193 (2016).
35. X. Xiong, T. Panchenko, S. Yang, S. Zhao, P. Yan, W. Zhang, W. Xie, Y. Li, Y. Zhao, C. D. Allis, H. Li, Selective recognition of histone crotonylation by double PHD fingers of MOZ and DPF2. *Nat. Chem. Biol.* **12**, 1111–1118 (2016).
36. D. Zhao, H. Guan, S. Zhao, W. Mi, H. Wen, Y. Li, Y. Zhao, C. D. Allis, X. Shi, H. Li, YEATS2 is a selective histone crotonylation reader. *Cell Res.* **26**, 629–632 (2016).
37. X. Ren, Y. Zhou, Z. Xue, N. Hao, Y. Li, X. Guo, D. Wang, X. Shi, H. Li, Histone benzoylation serves as an epigenetic mark for DPF and YEATS family proteins. *Nucleic Acids Res.* **49**, 114 (2020).
38. T. Tsusaka, M. A. Najar, B. Schwarz, E. Bohrnsen, J. A. Oses-Prieto, C. Lee, A. L. Burlingame, C. M. Bosio, G. M. Burslem, E. L. Goldberg, Reversible histone deacetylase activity catalyzes lysine acylation. bioRxiv 567549 [Preprint] (2023).
39. M. D. Asmamaw, A. He, L.-R. Zhang, H.-M. Liu, Y. Gao, Histone deacetylase complexes: Structure, regulation and function. *Biochim. Biophys. Acta Rev. Cancer* **1879**, 189150 (2024).
40. L. Chen, H. Deng, H. Cui, J. Fang, Z. Zuo, J. Deng, Y. Li, X. Wang, L. Zhao, Inflammatory responses and inflammation-associated diseases in organs. *Oncotarget* **9**, 7204–7218 (2018).
41. D. Furman, J. Campisi, E. Verdin, P. Carrera-Bastos, S. Targ, C. Franceschi, L. Ferrucci, D. W. Gilroy, A. Fasano, G. W. Miller, A. H. Miller, A. Mantovani, C. M. Weyand, N. Barzilai, J. J. Goronzy, T. A. Rando, R. B. Effros, A. Lucia, N. Kleinstreuer, G. M. Slavich, Chronic inflammation in the etiology of disease across the life span. *Nat. Med.* **25**, 1822–1832 (2019).
42. H. C. B. Nguyen, M. Adlanmerini, A. K. Hauck, M. A. Lazar, Dichotomous engagement of HDAC3 activity governs inflammatory responses. *Nature* **584**, 286–290 (2020).
43. Z. Wu, Y. Bai, Y. Qi, C. Chang, Y. Jiao, Y. Bai, Z. Guo, HDAC1 disrupts the tricarboxylic acid (TCA) cycle through the deacetylation of Nur77 and promotes inflammation in ischemia-reperfusion mice. *Cell Death Discov.* **9**, 10 (2023).
44. Y. Zeng, R. He, Y. Liu, T. Luo, Q. Li, Y. He, M. Fang, T. Wang, HDAC1 regulates inflammation and osteogenic differentiation of ankylosing spondylitis fibroblasts through the Wnt-Smad signaling pathway. *J. Orthop. Surg. Res.* **17**, 343 (2022).
45. L. Chen, W. Fischle, E. Verdin, W. C. Greene, Duration of nuclear NF-κB action regulated by reversible acetylation. *Science* **293**, 1653–1657 (2001).
46. B. P. Ashburner, S. D. Westerheide, A. S. Baldwin, The p65 (RelA) subunit of NF-κB interacts with the histone deacetylase (HDAC) corepressors HDAC1 and HDAC2 to negatively regulate gene expression. *Mol. Cell. Biol.* **21**, 7065–7077 (2001).
47. B. Huang, X.-D. Yang, M.-M. Zhou, K. Ozato, L.-F. Chen, Brd4 coactivates transcriptional activation of NF-κB via specific binding to acetylated RelA. *Mol. Cell. Biol.* **29**, 1375–1387 (2009).
48. "Potassium sorbate market analysis: Industry market size, plant capacity, production, operating efficiency, demand & supply gap, grade, end-user industries, sales channel, regional demand, company share, manufacturing process, 2015-2034" (ChemAnalyst, 2024); www.chemanalyst.com/industry-report/potassium-sorbate-market-3073.
49. L. Qiang, H. Xiao, E. I. Campos, V. C. Ho, G. Li, Development of a PAN-specific, affinity-purified anti-acetylated lysine antibody for detection, identification, isolation, and intracellular localization of acetylated protein. *J. Immunoassay Immunochem.* **26**, 13–23 (2005).
50. Z. Cheng, Y. Tang, Y. Chen, S. Kim, H. Liu, S. S. C. Li, W. Gu, Y. Zhao, Molecular characterization of propionyllysines in non-histone proteins. *Mol. Cell. Proteomics* **8**, 45–52 (2009).
51. A. A. Bachmanov, D. R. Reed, G. K. Beauchamp, M. G. Tordoff, Food intake, water intake, and drinking spout side preference of 28 mouse strains. *Behav. Genet.* **32**, 435–443 (2002).
52. D. Kim, J. M. Paggi, C. Park, C. Bennett, S. L. Salzberg, Graph-based genome alignment and genotyping with HISAT2 and HISAT-genotype. *Nat. Biotechnol.* **37**, 907–915 (2019).
53. Y.-C. Sin, M. Park, T. J. Griffin, J. Yong, Y. Chen, A constitutional isomer selective chemical proteomic strategy for system-wide profiling of protein lysine 5-hydroxylation. *Chem. Sci.* **15**, 18395–18404 (2024).
54. J. Cox, M. Mann, MaxQuant enables high peptide identification rates, individualized p.p.b.-range mass accuracies and proteome-wide protein quantification. *Nat. Biotechnol.* **26**, 1367–1372 (2008).
55. Z.-F. Yuan, S. Sidoli, D. M. Marchione, J. Simithy, K. A. Janssen, M. R. Szurgot, B. A. Garcia, EpiProfile 2.0: A computational platform for processing epi-proteomics mass spectrometry data. *J. Proteome Res.* **17**, 2533–2541 (2018).
56. D. Szklarczyk, A. L. Gable, K. C. Nastou, D. Lyon, R. Kirsch, S. Pyysalo, N. T. Doncheva, M. Legeay, T. Fang, P. Bork, L. J. Jensen, C. von Mering, The STRING database in 2021: Customizable protein-protein networks, and functional characterization of user-uploaded gene/measurement sets. *Nucleic Acids Res.* **49**, D605–D612 (2021).
57. P. Shannon, A. Markiel, O. Ozier, N. S. Baliga, J. T. Wang, D. Ramage, N. Amin, B. Schwikowski, T. Ideker, Cytoscape: A software environment for integrated models of biomolecular interaction networks. *Genome Res.* **13**, 2498–2504 (2003).
58. G. D. Bader, C. W. V. Hogue, An automated method for finding molecular complexes in large protein interaction networks. *BMC Bioinformatics* **4**, 2 (2003).
59. S. X. Ge, D. Jung, R. Yao, ShinyGO: A graphical gene-set enrichment tool for animals and plants. *Bioinformatics* **36**, 2628–2629 (2020).
60. G. E. Crooks, G. Hon, J.-M. Chandonia, S. E. Brenner, WebLogo: A sequence logo generator. *Genome Res.* **14**, 1188–1190 (2004).
61. Y. Perez-Riverol, J. Bai, C. Bandla, D. García-Seisdedos, S. Hewapathirana, S. Kamatchinathan, D. J. Kundu, A. Prakash, A. Frericks-Zipper, M. Eisenacher, M. Walzer, S. Wang, A. Brazma, J. A. Vizcaíno, The PRIDE database resources in 2022: A hub for mass spectrometry-based proteomics evidences. *Nucleic Acids Res.* **50**, D543–D552 (2022).

Acknowledgments: We are very grateful for the discussion and suggestions from the members of the Chen lab and helpful advice from D. Bernlohr and T. Griffin. We greatly appreciate Y. Zhao and P. Villalta from the mass spectrometry resource center in the Masonic Cancer Center at the University of Minnesota for LC-MS setup and access. **Funding:** Y.C. and D.G.M. were supported by funding from the University of Minnesota and the University Faculty Research Grant (21SFR-2YR150YC) from the Healthy Food Healthy Lives Institute at the University of Minnesota. J.E.G. was supported by funding from the National Institute of Health

(R01GM146386-03-S1), and J.L.H. was supported by funding from the College of Biological Sciences and the University of Minnesota Foundation Human Diseases Research Fund. **Author contributions:** Conceptualization: Y.-C.S., Y.C., and D.G.M. Methodology: Y.-C.S., Y.C., D.G.M., Z.-f.Y., and J.L.H. Software: Z.-f.Y. and Y.-C.S. Validation: Y.-C.S., B.A., Y.C., and D.G.M. Formal analysis: Y.-C.S., B.A., Y.C., and D.G.M. Resources: Y.C., D.G.M., and L.L.P. Data curation: Y.-C.S., B.A., Z.-f.Y., Y.C., and D.G.M. Investigation: Y.-C.S., B.A., Z.-f.Y., J.L.H., and J.E.G. Visualization: Y.-C.S. and Y.C. Supervision: Y.C., D.G.M., and L.L.P. Project administration: Y.C., D.G.M., L.L.P., and J.L.H. Writing—original draft: Y.C., D.G.M., and Y.-C.S. Writing—review and editing: Y.C., D.G.M., Y.-C.S., Z.-f.Y., and J.L.H. Funding acquisition: Y.C., D.G.M., and L.P. **Competing interests:** The authors declare that they have no competing interests. **Data and materials availability:** All data needed to evaluate the conclusions in the paper are present in the paper and/or the Supplementary Materials. The mass spectrometry proteomics data have been deposited to the ProteomeXchange Consortium via the PRIDE partner repository with the dataset identifier PXD058007 (www.ebi.ac.uk/pride/archive/projects/PXD058007) (*61*).

Submitted 5 December 2024
Accepted 25 April 2025
Published 30 May 2025
10.1126/sciadv.adv1071